

Preparation of fluorescent and antibacterial nanocomposite films based on cellulose nanocrystals/ZnS quantum dots/polyvinyl alcohol

Wei-Qi Xie · Kong-Xian Yu · Yi-Xian Gong

Received: 27 August 2018 / Accepted: 1 January 2019 / Published online: 4 January 2019
© Springer Nature B.V. 2019

Abstract In this paper, a fluorescent and antibacterial nanocomposite film based on Zinc sulphide (ZnS) quantum dots, cellulose nanocrystals (CNCs) and polyvinyl alcohol (PVA) was successfully synthesized. CNCs were first decorated in situ with ZnS quantum dots, which were then introduced into a PVA matrix to prepare nanocomposite films with good fluorescent and antibacterial properties. The X-ray diffraction and scanning electron microscope analysis indicated that ZnS nanoparticles were well-dispersed

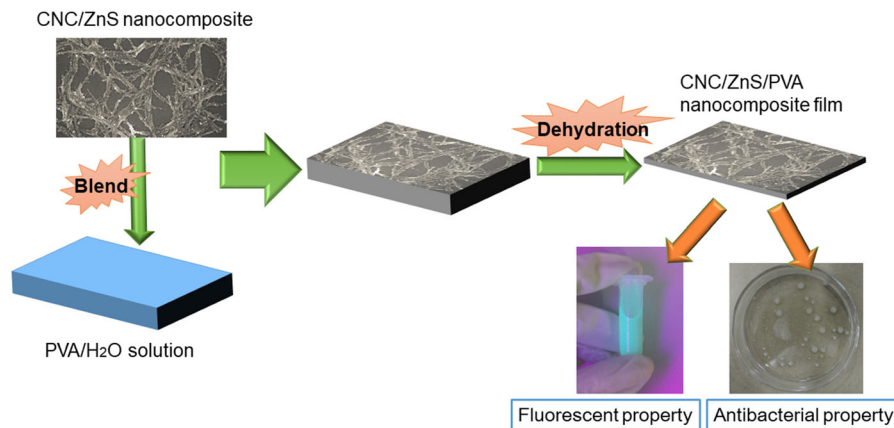
and randomly coated on the CNCs with uniform particle size. The visible emission peak in the ZnS/CNCs nanocomposites was 473 nm with an excitation wavelength of 350 nm. The CNCs loaded with ZnS quantum dots exhibited bright blue fluorescence under the ultraviolet light. Additionally, CNCs/ZnS nanocomposite films also had good antibacterial properties (bacterial inhibition rate = 78.25%).

W.-Q. Xie (✉)
School of Materials Science and Engineering, South
China University of Technology, Guangzhou, China
e-mail: mswqxie@mail.scut.edu.cn

W.-Q. Xie · Y.-X. Gong
State Key Laboratory of Pulp and Paper Engineering,
South China University of Technology, Guangzhou,
China

K.-X. Yu
Health Supervision Bureau of Liaoning Province,
Shenyang, China

Graphical abstract



Keywords ZnS quantum dots · Cellulose nanocrystals · Fluorescent · Nanocomposite film · Antibacterial properties

Introduction

In the recent years, the worldwide environmental pollution and resources shortage have attracted considerable attention (Xue et al. 2017; Zheng et al. 2016; Ma et al. 2016). Therefore, considerable research efforts have been aimed at developing environmentally friendly and green materials derived from the renewable resources (Arevalo-Gallegos et al. 2017; Ramesh et al. 2017; Dubey et al. 2017; Colmenares et al. 2016; Doudin et al. 2016). Cellulose nanocrystals (CNCs), highly crystalline nanomaterials that can be obtained from the renewable plants, have been widely used in composite reinforcements, nanomaterials, and flexible electronics (Geng et al. 2016; Jin et al. 2016; Molnes et al. 2016; Miao and Hamad 2016a, b). Its abundant reserves, recyclability, good biocompatibility and good mechanical properties, and nano-size effects make it one of the most useful bio-based materials (Lizundia et al. 2016; Chen et al. 2016; da Silva Souza et al. 2016).

Quantum dots (QDs) are one kind of small crystals with good fluorescence performance, long fluorescence lifetime, and continuous excitation spectrum (Lyons et al. 2017; Zhang et al. 2017; Lai et al. 2017). Among them, ZnS is one of the most used wide band gap fluorescence materials and is widely applied for

various applications (i.e., sensing material, solar cell and light-emitting diode) due to its many excellent properties (i.e., good optical properties, wide forbidden band gap and low toxicity) (Bwatanglang et al. 2016; Chantada-Vázquez et al. 2016; Li et al. 2013; Chuang et al. 2014).

Currently, many works have been reported on the synthesis of the ZnS QDs based nanocomposites (Xiao et al. 2014; Bruno et al. 2013; Wang et al. 2004). Some studies that focus on the effective dispersion of the ZnS QDs and retaining the original properties of the ZnS QDs have also been reported (Niu et al. 2014; Luna-Martinez et al. 2011; Chang et al. 2009). Niu et al. (2014) prepared ZnS/cellulose composites by blending natural cellulose nanofibers with ZnS QDs with the hydrothermal method. Luna-Martínez et al. (2011) reported that ZnS/sodium carboxymethyl cellulose nanocomposites and films with fluorescence properties were synthesized by blending ZnS nanoparticles with sodium carboxymethyl cellulose in situ; Chang et al. (2009) prepared CdSe/ZnS/cellulose hydrogels by the chemical cross-linking method. CNCs, which are extracted from plants by controlled acid hydrolysis and has many beneficial properties, could be a potential biomaterial for the preparation of CNCs/ZnS QD nanocomposites in situ (Ng et al. 2015; Cheung et al. 2013; Valentini et al. 2013; Zhu et al. 2014).

In this paper, we investigated a fluorescent nanocomposite film based on ZnS QD-decorated CNCs with the in situ hydrothermal method. This present preparation method is simple and does not require additional surface modification. The

fluorescence properties of QDs were investigated by means of Fourier transform infrared spectrophotometer (FT-IR), X-ray diffraction (XRD), X-ray photoelectron spectroscopy (XPS), scanning electron microscope (SEM), and photoluminescence spectroscopy (PL). Polyvinyl alcohol (PVA) is a biocompatible, water-soluble synthetic polymer with excellent film forming and mechanical properties, which has been widely used as the matrix for preparing CNC based composites (Niu et al. 2015). PVA can also form strong interactions with CNCs via hydrogen bonding (Zheng et al. 2013). In this work, by blending the CNCs/ZnS composites with PVA, the CNCs/ZnS/PVA composite films can be synthesized. In addition, the mechanical, fluorescent, and antibacterial properties of the CNCs/ZnS/PVA composite films were also studied.

Experimental

Materials

All chemicals used in this research, including sulphuric acid (H_2SO_4), PVA, zinc chloride (ZnCl), sodium sulfide (NaS) and polyethyleneimine (PEI) were analytical grade and purchased from a chemical supplier (Shanghai Macklin Co., Ltd. (Shanghai, China)). Microcrystalline cellulose was used as the raw material and obtained from a chemical supplier (Sigma–Aldrich, USA). High purity Millipore water was used in this study.

Synthesis and purification of CNCs (Jin et al. 2016; Luna-Martinez et al. 2011)

60 mL of 64% sulfuric acid was added into a beaker and heated at 45 °C using water bath, and then 6 g dried microcrystalline cellulose was added in the beaker and stirred for 40 min. After that, the obtained suspension was poured into a 600 mL beaker that contains distilled water and then left standing for 8 h. Afterward, the suspension was transferred to a centrifuge (rotational speed = 10,000 r/min, temperature = 25 °C) for 15 min, and then the supernatant was removed. The above operation was repeated several times. The obtained suspensions (CNCs) were collected and then neutralized by dialysis (final pH

value = 7). Finally, The CNCs were stored in erlenmeyer flask at 4 °C.

Preparation of the CNCs/ZnS nanocomposites

The CNCs/ZnS nanocomposites were prepared by using the hydrothermal method. 0.500 g of polyethyleneimine (PEI), 0.136 g of zinc chloride (ZnCl), 0.078 g of NaS and 70 mL homogeneous prepared CNCs were added into a beaker (100 mL), after stirring for 30 min, the mixture solution was poured into a hydrothermal reactor and heated at 180 °C for 8 h. After the reaction completed, the mixture solution was cooled to room temperature and then yellow dispersion with no apparent sediment was obtained. Thus, the CNCs/ZnS nanocomposite was synthesized. The partial suspension was freeze-dried for the subsequent testing and the remaining dispersion was stored in erlenmeyer flask at 4 °C.

Preparation of CNCs/ZnS/PVA nanocomposite film

For the preparation of the CNCs/ZnS/PVA nanocomposite films, a predetermined amount of CNCs/ZnS suspension was mixed with the PVA. PVA (2.0 g) was dissolved in the prepared CNCs/ZnS suspension with vigorous stirring at 90 °C. After PVA was completely dissolved in the suspension, the mixture solutions were poured onto a polytetrafluoroethylene Petri dish with a diameter of 10 cm, and then were dried in the vacuum oven at 60 °C for 48 h. CNCs/ZnS/PVA nanocomposite films with 1, 2, 3, 4 and 5 wt% of CNCs/ZnS composites were prepared and coded as C-1, C-2, C-3, C-4 and C-5, respectively. Thus, the CNCs/ZnS/PVA nanocomposite films were obtained. Figure 1 shows the synthesis procedures of the CNCs/ZnS/PVA nanocomposite film that contains ZnS QDs.

Characterizations and measurements

The infrared spectra of CNCs and CNCs/ZnS nanocomposite were recorded using FT-IR (Nicole, NEXUS 670). The sample was ground and mixed with dried potassium bromide (KBr) powder and compressed, and then was subjected to analysis. The experiments were performed in the range of 400–4000 cm^{-1} for each sample. The resolution and scanning time were 4 cm^{-1} and 32 times, respectively.

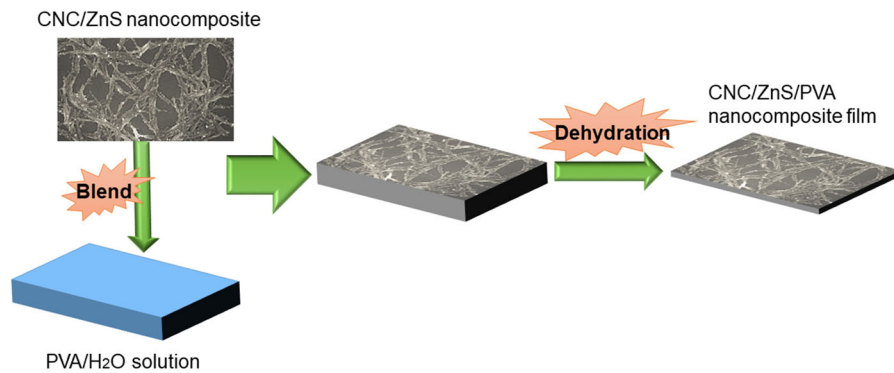


Fig. 1 Synthesis procedures of the CNCs/ZnS/PVA nanocomposite film

The UV–vis spectra and the transmittance of CNCs/ZnS/PVA nanocomposite films were recorded using UV–vis absorption spectroscopy (Shimadzu, UV-1800). The photoluminescence (PL) characterizations of samples were performed using a FluoroMax-4 fluorescence spectrometer.

The morphology of CNCs and CNCs/ZnS nanocomposites were evaluated by scanning electron microscope (SEM, LEO 153 VP). A freeze-dried CNCs/ZnS composite was coated with gold palladium by a PolaronE 5100 coater and then analyzed with an accelerating voltage of 5 kV.

The elastic modulus and tensile strength of CNCs/ZnS/PVA nanocomposite films were tested by using a universal testing instrument (Instron5565 Material Test System). The dimensions of the samples to be measured were 15.0 mm width and 50.0 mm length.

XRD patterns of the samples were identified by a Rigaku D/max-1200 X-ray diffractometer with a Cu-K α radiation, and the step scanning was done at a scanning rate of 2°/s ranging from 4° to 70° (2 h angle).

XPS analysis was performed by using Kratos Axis Ultra DLD. The X light source (Mono AlK α) at the energy of 1486.6 eV was used, with a beam spot size of 700 × 300 μ m, a full spectrum scanning energy of 160 eV, and a narrow spectrum scanning energy of 40 eV.

The antibacterial activity of CNCs/ZnS/PVA nanocomposite film against *Escherichia coli* (*E. coli*) were assessed by the bacterial inhibition rate method (Sawai 2003; Zhang and Xiao 2013). 9.0 mL of 0.03 mol/L phosphate buffered saline (PBS) solution was added in a flask containing 1.0 mL of *E. coli* solution, and 0.2 g of CNCs/ZnS/PVA nanocomposite

film (CNCs/ZnS content = 3%) or blank film (pure PVA film) was placed into the above flask. Afterward, the flask was immersed in a water bath shaker and shaken at 37 °C for 1 h. 0.2 mL of each solution was added and seeded on an agar culture medium (in petri dish), and then the petri dish was placed in an incubator and incubated at 37 °C for 24 h. The bacteria concentration in the petri dish was calculated before and after 24 h of incubation, and then the bacterial inhibition rate can be obtained. The number of colonies was recorded. The bacteria concentration can be calculated by the following equation:

$$K = Z \times R \quad (1)$$

where K represents the concentration of bacteria (CFU/mL) in each sample, Z represents the average number of two plate colonies and R represents the dilution factor.

The bacterial inhibition rate against *E. coli* can be calculated as:

$$Y = \frac{K_t - K_0}{K_t} \times 100\% \quad (2)$$

where Y, K_t and K₀ represent the bacterial inhibition rate of the film sample, the concentration of bacteria (CFU/mL) in CNCs/ZnS/PVA nanocomposite film sample and the blank sample (pure PVA film without adding CNCs/ZnS) after 24 h of incubation, respectively.

Results and discussion

Characterization of the CNCs/ZnS nanocomposites

FTIR characterization

In order to study the structural characteristics of CNCs and CNCs/ZnS nanocomposites and the interaction between ZnS and CNCs, FTIR testing were conducted. Figure 2 showed the FTIR spectra of the CNCs and ZnS/CNCs nanocomposites. It can be seen that the peak at 3415 cm^{-1} , corresponding to the -OH stretching vibrational absorption (Zhao et al. 2014), moved slightly to the higher wavenumber (3428 cm^{-1}). The data indicated that the hydroxyl groups (-OH) was the active sites in the CNCs/ZnS nanocomposite preparation and there was an interaction between -OH and ZnS QDs. The peaks at 1639 and 1060 cm^{-1} , corresponding respectively to the C=O and C-O-C stretching vibrational absorption (Dong et al. 2012), moved slightly to the lower wavenumbers (1632 and 1057 cm^{-1} respectively). However, the peak at 1429 cm^{-1} , corresponding to the stretching vibrational absorption of $\text{-CH}_2\text{-}$ (Cao et al. 2014), moved to the higher wavenumber (1461 cm^{-1}), which also indicated the interaction between CNCs and ZnS QDs.

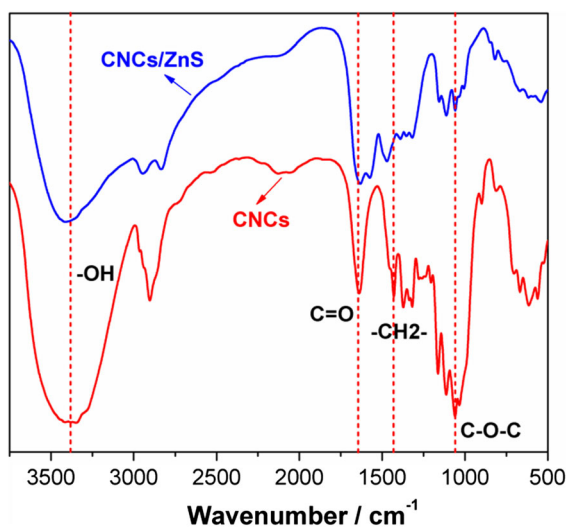


Fig. 2 FT-IR spectra of CNCs and CNCs/ZnS nanocomposites

XRD analysis

The crystal structures of the CNCs and CNCs/ZnS nanocomposite were analyzed by XRD. Figure 3 showed the XRD patterns of pure CNCs and CNCs/ZnS nanocomposite. There were three broad peaks (2θ) at about 15.0° , 16.5° and 22.5° in the pattern of CNCs, which were assigned to the (1–10), (110) and (200) plane in CNCs (i.e., cellulose I β) crystalline structure, respectively (French 2014). In addition, three similar XRD diffraction peaks can be observed in the pattern of the CNCs/ZnS nanocomposite. The typical cellulose crystalline structure of CNCs/ZnS nanocomposite showed that the structure of CNCs in CNCs/ZnS were not destroyed under the conditions of the in situ hydrothermal method. The other diffraction peaks of CNCs/ZnS nanocomposite were at 28.6° , 47.8° , and 56.7° , which correspond to the crystal planes of the (1 1 1), (2 2 0) and (3 1 1) of the cubic structure of ZnS (JPDS: 65-9585), respectively (Leng et al. 2014). The results showed that the ZnS QDs were loaded on the CNCs matrix, and the newly generated QDs exhibited a true crystalline structure.

XPS analysis

The XPS analysis was carried out to obtain the information about the related functional groups of CNCs/ZnS nanocomposites. The peaks of the related atoms (O, C, S, Zn, and N) in the nanocomposites were observed in the XPS spectra are illustrated in Fig. 4a.

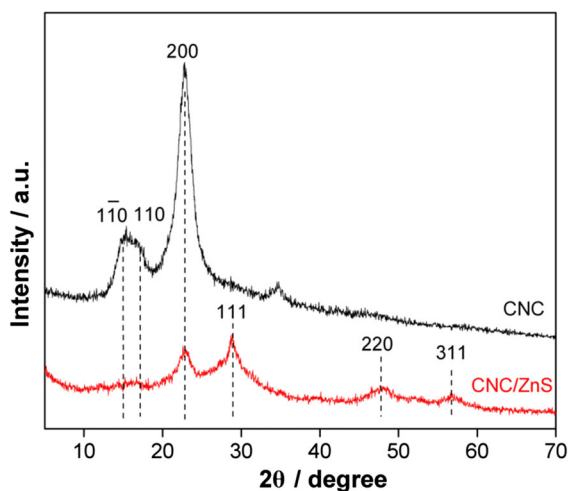


Fig. 3 XRD spectra of CNCs and CNCs/ZnS nanocomposites

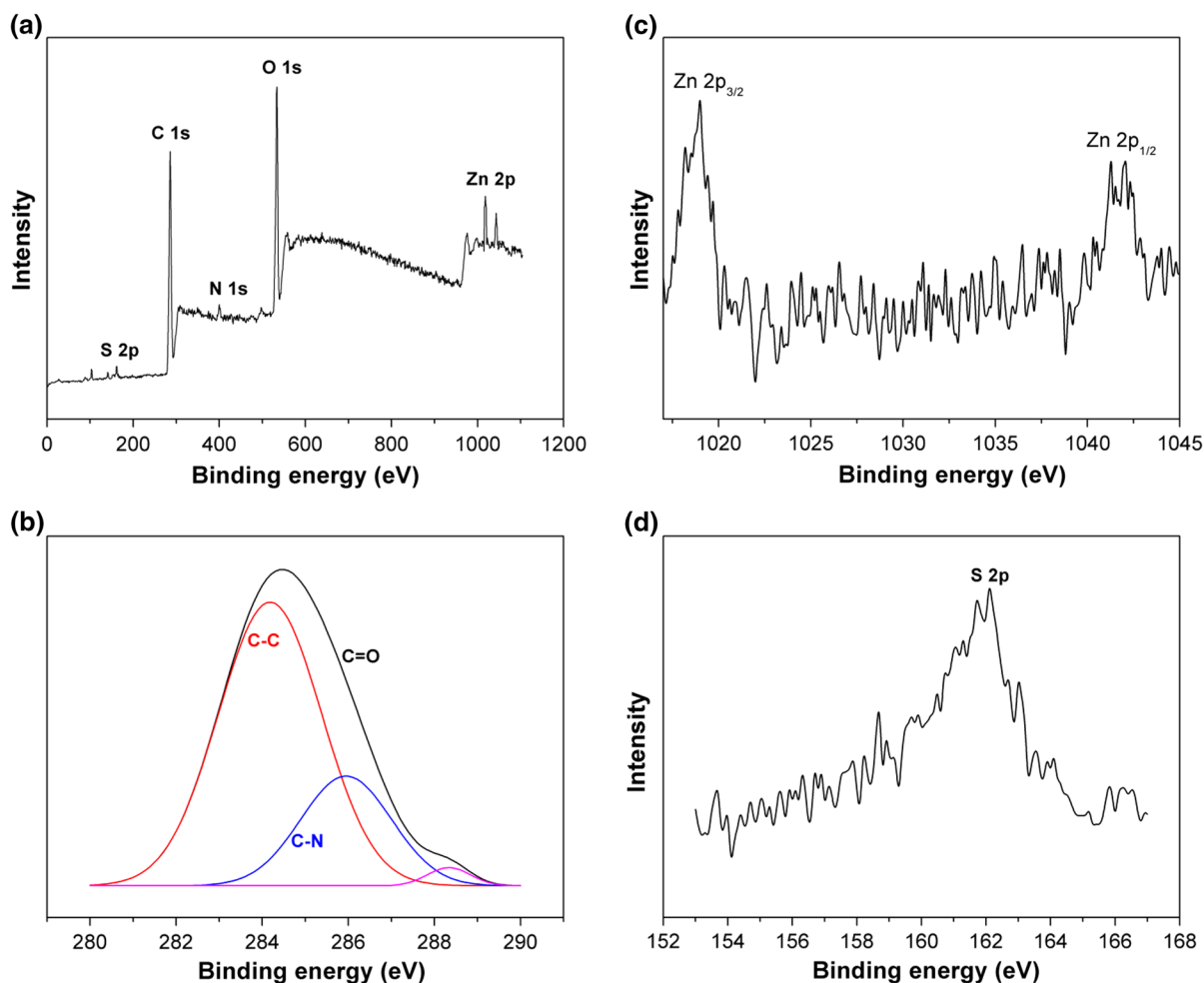


Fig. 4 **a** XPS spectrum of CNCs/ZnS nanocomposite; **b** high-resolution XPS scan for C 1s of CNCs/ZnS nanocomposite; **c** high-resolution XPS scan for Zn 2p of CNCs/ZnS nanocomposite; **d** high-resolution XPS scan for S 2p of CNCs/ZnS nanocomposite

The signal of nitrogen (N 1s) indicated that the existence of PEI in the CNCs/ZnS nanocomposites was confirmed (Stankovich et al. 2006). PEI was used to improve the stability and promote adhesion to the negatively charged surface of CNCs/ZnS nanocomposites (Gu et al. 2010). Figure 4b illustrated the C 1s XPS spectra of CNCs/ZnS nanocomposites, which proved that the existence of three kinds of carbons: C–C (284.2 eV), C–N (285.9 eV), and C=O (288.3 eV) was confirmed, indicating that PEI was successfully grafted to CNCs (Johansson et al. 2005). The Zn 2p XPS spectra of CNCs/ZnS nanocomposites in Fig. 4c showed the exhibition of Zn 2p_{3/2} and Zn 2p_{1/2} peaks, and the binding energies of the two peaks were at 1019 eV and 1043 eV, respectively, indicating the characteristic peaks of Zn ions in CNCs/ZnS

nanocomposites. The S 2p XPS spectrum of CNCs/ZnS nanocomposites in Fig. 4d showed the exhibition of S 2p peak, and the binding energy of this peak was at 162.1 eV, which indicated the characteristic peaks of S²⁻ in CNCs/ZnS nanocomposites.

SEM

The morphology images of CNCs/ZnS nanocomposites were characterized by SEM. From Fig. 5a we can find the three-dimensional (3D) porous network structure of CNCs. This mesoporous structure provides a good tunnel for the adsorption of Zn²⁺, so that Zn²⁺ is uniformly distributed on the CNCs. Figure 5b showed the SEM image of CNCs/ZnS nanocomposites and can be seen that ZnS QDs were well-dispersed and

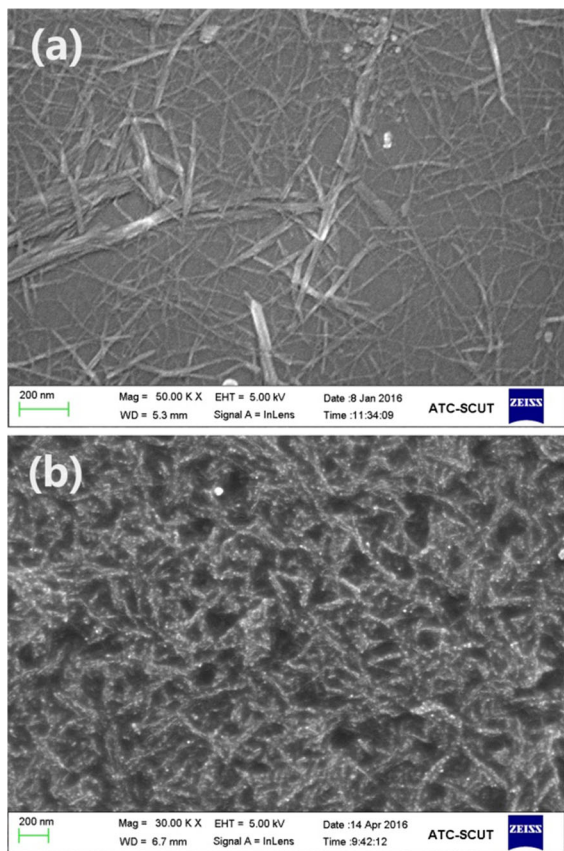


Fig. 5 SEM images of **a** CNCs and **b** CNCs/ZnS nanocomposites

randomly coated on the CNCs with uniform particle size and the particle diameter of QDs in the CNCs/ZnS nanocomposites was approximately 15 nm.

Fluorescence properties of CNCs/ZnS nanocomposites and CNCs/ZnS/PVA nanocomposite films

The PL properties of CNCs and CNCs/ZnS composites were measured by a fluorescence spectrophotometer (excitation wavelength = 350 nm). As illustrated in Fig. 6, a visible emission peak was occurred at 473 nm in the PL spectrum of the ZnS/CNCs nanocomposites. The PL spectrum of the ZnS/CNCs nanocomposites also had a broad fluorescent emission spectral band. However, there were no emission peaks in the PL spectrum of original CNCs, which indicated that the structure of CNCs are a suitable substrate for the assembly of ZnS QDs.

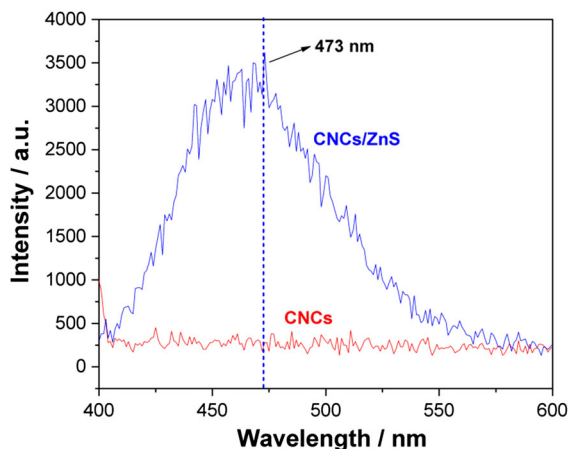


Fig. 6 Fluorescence spectra of CNCs and CNCs/ZnS nanocomposites

Figure 7 showed the reflection of the CNCs/ZnS nanocomposites under the irradiation of the fluorescent lamp and the ultraviolet lamp. It can be seen that a light yellow color can be observed in the CNCs/ZnS nanocomposites under the irradiation of fluorescent lamp, and a bright blue fluorescence can be observed under the irradiation of ultraviolet lamp. The decorated CNCs/ZnS particles were added to PVA to form CNC/ZnS/PVA composite films. The fluorescence properties of CNCs/ZnS/PVA nanocomposite films were also studied. Figure 8 showed the fluorescence spectra of CNCs/ZnS/PVA composite films with different CNCs/ZnS additions (an excitation wavelength of 350 nm and a slit of 1 nm), from which can be seen that the fluorescence intensity increased with

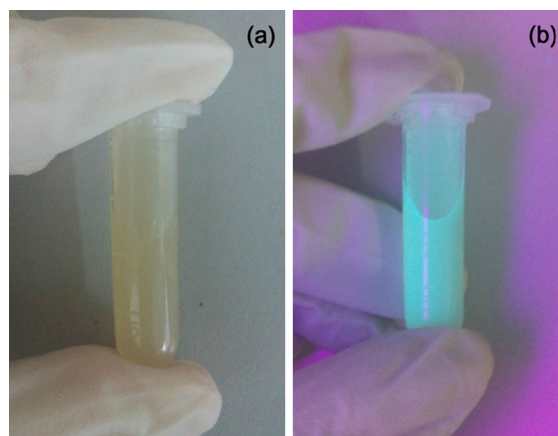


Fig. 7 CNCs/ZnS nanocomposites under **a** the fluorescent light and **b** ultraviolet light. (Color figure online)

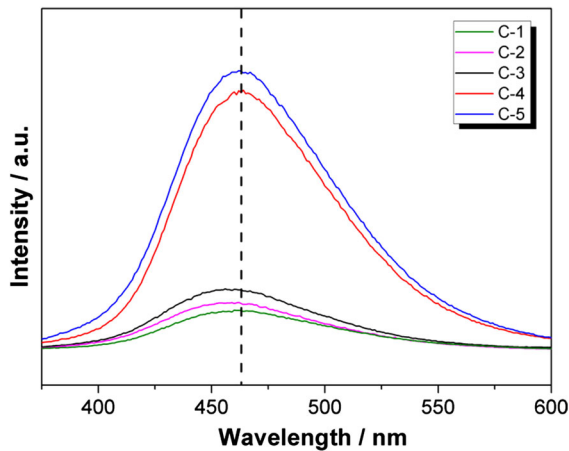


Fig. 8 Fluorescence spectra of CNCs/ZnS/PVA nanocomposite films

the increase of the CNCs/ZnS nanocomposite content. The increasing trend was more obvious when the content of the CNCs/ZnS nanocomposite reached 4%.

Light transmittance of CNCs/ZnS/PVA nanocomposite films

The light transmittance of CNCs/ZnS/PVA nanocomposite films was assessed by the UV–vis spectroscopy. Figure 9 showed the light transmittance of CNCs/ZnS/PVA nanocomposite films with different CNCs/ZnS contents. As seen, the light transmittance of the CNCs/ZnS/PVA nanocomposite films decreased with the increase of the CNCs/ZnS content and were below 40%. According to the previous papers (Moon et al.

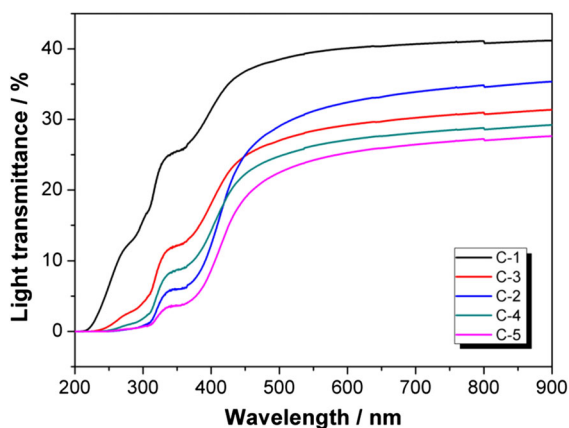


Fig. 9 Light transmittance of of CNCs/ZnS/PVA nanocomposite films

2013; Araki et al. 2014), the decrease of the transparency may be due to the high haze of the films.

Mechanical properties of CNCs/ZnS/PVA nanocomposite films

The mechanical properties (elastic modulus and tensile strength) of the CNCs/ZnS/PVA nanocomposite films were measured by a universal testing instrument. All testing were repeated for four time. Figure 10a and b showed the effect of CNCs/ZnS nanocomposite content on the elastic modulus and tensile strength of CNCs/ZnS/PVA films, respectively. From which can be seen that the elastic modulus of the films gradually increased with the increase of the CNCs/ZnS content. The tensile

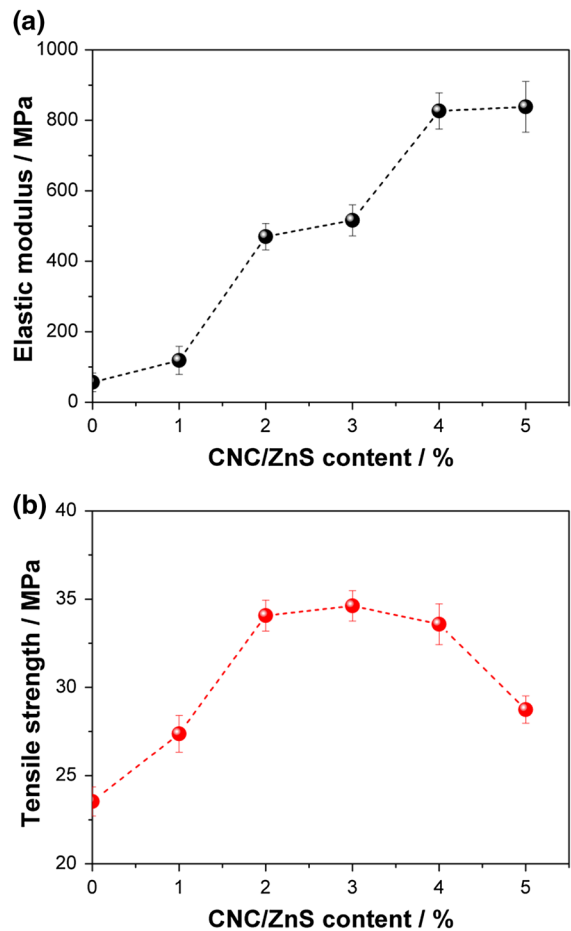


Fig. 10 **a** Elastic modulus of CNCs/ZnS/PVA nanocomposite films; **b** Tensile strength of CNCs/ZnS/PVA nanocomposite films

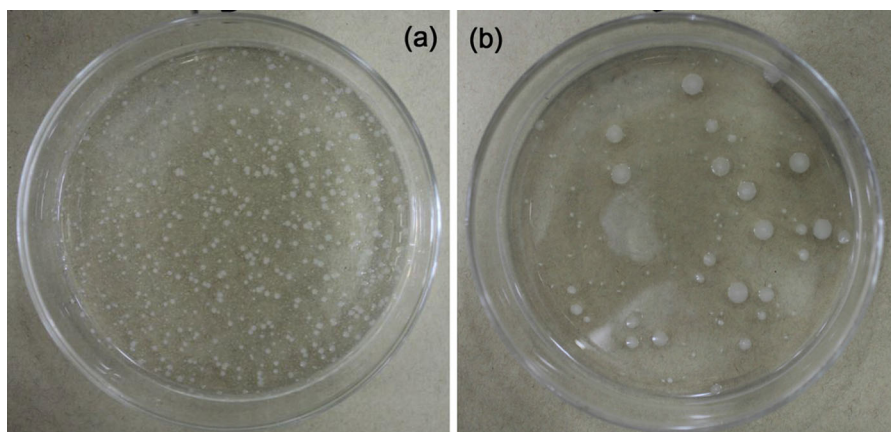


Fig. 11 **a** Photo images of bacterial colonies formed by *E. coli* on blank (without CNCs/ZnS composites) sample and **b** CNCs/ZnS/PVA nanocomposite film sample

strength of the nanocomposite films increased at first, and then had a decrease trend after the addition of CNCs/ZnS nanocomposites reached 3%. The reason for the decrease in tensile strength may be that the CNCs suspensions flocculate more easily when the CNCs content increase.

Antibacterial properties of CNCs/ZnS/PVA nanocomposite film

The bacterial inhibition rate was used to measure the antibacterial activity of CNCs/ZnS/PVA composite film (CNCs/ZnS content = 4%). After 24 h of incubation (at 37 °C), the bacteria concentration in the CNCs/ZnS/PVA composite film sample was compared with that of the blank sample (pure PVA film without adding CNCs/ZnS). Figure 11a and b showed the bacterial colonies formed by *E. coli* in the blank sample and CNCs/ZnS/PVA nanocomposite film sample, respectively. It can be seen that there were a large number of bacterial colonies on the blank sample (without CNCs/ZnS composites), while the number of bacterial colonies on the CNCs/ZnS/PVA nanocomposite film sample was greatly reduced. The results showed that the average number of bacterial colonies on the CNCs/ZnS/PVA nanocomposite film sample was 152, and the blank sample was 699. And then the bacterial inhibition rate of the CNCs/ZnS/PVA nanocomposite film can be calculated by using Eq. (2) and is 78.25%, which indicated that the CNCs/ZnS/PVA nanocomposite film had the

antibacterial effect on *E. coli*. In the CNCs/ZnS/PVA nanocomposite film, ZnS is one of the most stable zinc compounds and is much more stable than the organic fungicides. The electrostatic interaction between CNCs/ZnS/PVA and the bacterial cell membrane may be the major reason for the antibacterial effect of the nanocomposite film. In addition, the composite film had a large contact area with the *E. coli* due to the roughened surface of the film, which increased the surface adhesion and interaction between the film and *E. coli*, leading to better antibacterial properties of the CNCs/ZnS/PVA nanocomposite film.

Conclusions

In this study, a fluorescent and antibacterial nanocomposite film based on CNCs/ZnS QDs was successfully prepared. The unique 3D porous structures of CNCs make CNCs the effective nanoreactor for the in situ preparation of ZnS nanoparticles. The results from XRD and SEM indicated that ZnS QDs were well-dispersed on the CNCs through adsorption of the cationic fixing agent PEI. The CNCs/ZnS/PVA nanocomposite film had a smooth PL spectrum, which indicated that the nanocomposite film had few impurities and good fluorescence properties. The CNCs loaded with ZnS QDs exhibited bright blue fluorescence under the UV light. The CNCs/ZnS/PVA nanocomposite films also showed good antibacterial properties (bacterial inhibition rate = 78.25%).

Acknowledgments The authors acknowledge the financial support from the State Key Laboratory of Pulp and Paper Engineering, South China University of Technology, China.

References

- Araki T, Jiu J, Nogi M, Koga H, Nagao S, Sugahara T, Suganuma K (2014) Low haze transparent electrodes and highly conducting air dried films with ultra-long silver nanowires synthesized by one-step polyol method. *Nano Res* 7(2):236–245
- Arevalo-Gallegos A, Ahmad Z, Asgher M, Parra-Saldivar R, Iqbal HM (2017) Lignocellulose: a sustainable material to produce value-added products with a zero waste approach—a review. *Int J Biol Macromol* 99:308–318
- Bruno A, Borriello C, Di Luccio T, Nenna G, Sessa L, Haque SA, Minarini C (2013) White light-emitting nanocomposites based on an oxadiazole–carbazole copolymer (POC) and InP/ZnS quantum dots. *J Nanopart Res* 15(11):2085
- Bwatanglang IB, Mohammad F, Yusof NA, Abdullah J, Hussein MZ, Alitheen NB, Abu N (2016) Folic acid targeted Mn: ZnS quantum dots for theranostic applications of cancer cell imaging and therapy. *Int J Nanomed* 11:413
- Cao L, Tang F, Fang G (2014) Preparation and characteristics of microencapsulated palmitic acid with TiO₂ shell as shape-stabilized thermal energy storage materials. *Sol Energy Mater Sol Cells* 123:183–188
- Chang C, Peng J, Zhang L, Pang DW (2009) Strongly fluorescent hydrogels with quantum dots embedded in cellulose matrices. *J Mater Chem* 19(41):7771–7776
- Chantada-Vázquez MP, Sánchez-González J, Peña-Vázquez E, Tabernero MJ, Bermejo AM, Bermejo-Barrera P, Moreda-Piñeiro A (2016) Synthesis and characterization of novel molecularly imprinted polymer-coated Mn-doped ZnS quantum dots for specific fluorescent recognition of cocaine. *Biosens Bioelectron* 75:213–221
- Chen L, Zhu JY, Baez C, Kitin P, Elder T (2016) Highly thermal-stable and functional cellulose nanocrystals and nanofibrils produced using fully recyclable organic acids. *Green Chem* 18(13):3835–3843
- Cheung CC, Giese M, Kelly JA, Hamad WY, MacLachlan MJ (2013) Iridescent chiral nematic cellulose nanocrystal/polymer composites assembled in organic solvents. *ACS Macro Lett* 2(11):1016–1020
- Chuang PH, Lin CC, Liu RS (2014) Emission-tunable CuInS₂/ZnS quantum dots: structure, optical properties, and application in white light-emitting diodes with high color rendering index. *ACS Appl Mater Interfaces* 6(17):15379–15387
- Colmenares JC, Varma RS, Lisowski P (2016) Sustainable hybrid photocatalysts: titania immobilized on carbon materials derived from renewable and biodegradable resources. *Green Chem* 18(21):5736–5750
- da Silva Souza DR, de Mesquita JP, Lago RM, Caminhas LD, Pereira FV (2016) Cellulose nanocrystals: a versatile precursor for the preparation of different carbon structures and luminescent carbon dots. *Ind Crop Prod* 93:121–128
- Dong Y, Shao J, Chen C, Li H, Wang R, Chi Y, Lin X, Chen G (2012) Blue luminescent graphene quantum dots and graphene oxide prepared by tuning the carbonization degree of citric acid. *Carbon* 50(12):4738–4743
- Doudin K, Al-Malaika S, Sheena HH, Tverezovskiy V, Fowler P (2016) New genre of antioxidants from renewable natural resources: synthesis and characterisation of rosemary plant-derived antioxidants and their performance in polyolefins. *Polym Degrad Stab* 130:126–134
- Dubey SP, Thakur VK, Krishnaswamy S, Abhyankar HA, Marchante V, Brighton JL (2017) Progress in environmental-friendly polymer nanocomposite material from PLA: synthesis, processing and applications. *Vacuum* 146:655–663
- French AD (2014) Idealized powder diffraction patterns for cellulose polymorphs. *Cellulose* 21(2):885–896
- Geng S, Haque MMU, Oksman K (2016) Crosslinked poly(vinyl acetate) (PVAc) reinforced with cellulose nanocrystals (CNC): structure and mechanical properties. *Compos Sci Technol* 126:35–42
- Gu Y, Niu T, Huang J (2010) Functional polymeric hybrid nanotubular materials derived from natural cellulose substances. *J Mater Chem* 20(45):10217–10223
- Jin E, Guo J, Yang F, Zhu Y, Song J, Jin Y, Rojas OJ (2016) On the polymorphic and morphological changes of cellulose nanocrystals (CNC-I) upon mercerization and conversion to CNC-II. *Carbohydr Polym* 143:327–335
- Johansson LS, Campbell JM, Fardim P, Hultén AH, Boisvert JP, Ernstsson M (2005) An XPS round robin investigation on analysis of wood pulp fibres and filter paper. *Surf Sci* 584(1):126–132
- Lai PY, Huang CC, Chou TH, Ou KL, Chang JY (2017) Aqueous synthesis of Ag and Mn co-doped In₂S₃/ZnS quantum dots with tunable emission for dual-modal targeted imaging. *Acta Biomater* 50:522–533
- Leng Z, Huang L, Shao F, Lv Z, Li T, Gu X, Han H (2014) Facile synthesis of Cu–In–Zn–S alloyed nanocrystals with temperature-dependent photoluminescence spectra. *Mater Lett* 119:100–103
- Li M, Zhou X, Guo S, Wu N (2013) Detection of lead (II) with a “turn-on” fluorescent biosensor based on energy transfer from CdSe/ZnS quantum dots to graphene oxide. *Biosens Bioelectron* 43:69–74
- Lizundia E, Fortunati E, Dominici F, Vilas JL, León LM, Armentano I, Torre L, Kenny JM (2016) PLLA-grafted cellulose nanocrystals: role of the CNC content and grafting on the PLA bionanocomposite film properties. *Carbohydr Polym* 142:105–113
- Luna-Martinez JF, Hernández-Uresti DB, Reyes-Melo ME, Guerrero-Salazar CA, González-González VA, Sepúlveda-Guzmán S (2011) Synthesis and optical characterization of ZnS–sodium carboxymethyl cellulose nanocomposite films. *Carbohydr Polym* 84(1):566–570
- Lyons TY, Williams DN, Rosenzweig Z (2017) Addition of fluorescence lifetime spectroscopy to the tool kit used to study the formation and degradation of luminescent quantum dots in solution. *Langmuir* 33(12):3018–3027
- Ma D, Chen W, Hu G, Zhang Y, Gao Y, Yin Y, Zhao Y (2016) K₂S₂O₈-mediated metal-free direct P–H/C–H functionalization: a convenient route to benzo [b] phosphole oxides from unactivated alkynes. *Green Chem* 18(12):3522–3526

- Miao C, Hamad WY (2016a) In-situ polymerized cellulose nanocrystals (CNC)—poly (l-lactide) (PLLA) nanomaterials and applications in nanocomposite processing. *Carbohydr Polym* 153:549–558
- Miao C, Hamad WY (2016b) Alkenylation of cellulose nanocrystals (CNC) and their applications. *Polymer* 101:338–346
- Molnes SN, Torrijos IP, Strand S, Paso KG, Syverud K (2016) Sandstone injectivity and salt stability of cellulose nanocrystals (CNC) dispersions—premises for use of CNC in enhanced oil recovery. *Ind Crop Prod* 93:152–160
- Moon IK, Kim JI, Lee H, Hur K, Kim WC, Lee H (2013) 2D graphene oxide nanosheets as an adhesive over-coating layer for flexible transparent conductive electrodes. *Sci Rep* 3:1112
- Ng HM, Sin LT, Tee TT, Bee ST, Hui D, Low CY, Rahmat AR (2015) Extraction of cellulose nanocrystals from plant sources for application as reinforcing agent in polymers. *Compos Part B Eng* 75:176–200
- Niu T, Xu J, Xiao W, Huang J (2014) Cellulose-based catalytic membranes fabricated by deposition of gold nanoparticles on natural cellulose nanofibres. *RSC Adv* 4(10):4901–4904
- Niu Y, Zhang X, He X, Zhao J, Zhang W, Lu C (2015) Effective dispersion and crosslinking in PVA/cellulose fiber bio-composites via solid-state mechanochemistry. *Int J Biol Macromol* 72:855–861
- Ramesh M, Palanikumar K, Reddy KH (2017) Plant fibre based bio-composites: sustainable and renewable green materials. *Renew Sust Energy Rev* 79:558–584
- Sawai J (2003) Quantitative evaluation of antibacterial activities of metallic oxide powders (ZnO, MgO and CaO) by conductimetric assay. *J Microbiol Methods* 54(2):177–182
- Stankovich S, Piner RD, Chen X, Wu N, Nguyen ST, Ruoff RS (2006) Stable aqueous dispersions of graphitic nanoplatelets via the reduction of exfoliated graphite oxide in the presence of poly (sodium 4-styrenesulfonate). *J Mater Chem* 16(2):155–158
- Valentini L, Cardinali M, Fortunati E, Torre L, Kenny JM (2013) A novel method to prepare conductive nanocrystalline cellulose/graphene oxide composite films. *Mater Lett* 105:4–7
- Wang D, He J, Rosenzweig N, Rosenzweig Z (2004) Superparamagnetic Fe₂O₃ beads–CdSe/ZnS quantum dots core–shell nanocomposite particles for cell separation. *Nano Lett* 4(3):409–413
- Xiao FX, Miao J, Liu B (2014) Layer-by-layer self-assembly of CdS quantum dots/graphene nanosheets hybrid films for photoelectrochemical and photocatalytic applications. *J Am Chem Soc* 136(4):1559–1569
- Xue XY, Cheng R, Shi L, Ma Z, Zheng X (2017) Nanomaterials for water pollution monitoring and remediation. *Environ Chem Lett* 15(1):23–27
- Zhang D, Xiao H (2013) Dual-functional beeswaxes on enhancing antimicrobial activity and water vapor barrier property of paper. *ACS Appl Mater Interfaces* 5(8):3464–3468
- Zhang Y, Xia J, Li C, Zhou G, Yang W, Wang D, Zheng H, Du Y, Li X, Li Q (2017) Near-infrared-emitting colloidal Ag₂S quantum dots excited by an 808 nm diode laser. *J Mater Sci* 52(16):9424–9429
- Zhao M, Deng C, Zhang X (2014) The design and synthesis of a hydrophilic core–shell–shell structured magnetic metal–organic framework as a novel immobilized metal ion affinity platform for phosphoproteome research. *Chem Commun* 50(47):6228–6231
- Zheng Q, Javadi A, Sabo R, Cai Z, Gong S (2013) Polyvinyl alcohol (PVA)–cellulose nanofibril (CNF)–multiwalled carbon nanotube (MWCNT) hybrid organic aerogels with superior mechanical properties. *RSC Adv* 3(43):20816–20823
- Zheng CW, Li CY, Pan J, Liu MY, Xia LL (2016) An overview of global ocean wind energy resource evaluations. *Renew Sust Energy Rev* 53:1240–1251
- Zhu H, Fang Z, Preston C, Li Y, Hu L (2014) Transparent paper: fabrications, properties, and device applications. *Energy Environ Sci* 7(1):269–287

Publisher's Note Springer Nature remains neutral with regard to jurisdictional claims in published maps and institutional affiliations.